Combination

of differential $D^{*\pm}$ cross-sections $d\sigma$ (*H1* & *ZEUS* data) in Deep-Elastic *ep* Scattering at HERA.

Jan Hladký, Institute of Physics, Acad.Sci., Czech Rep.

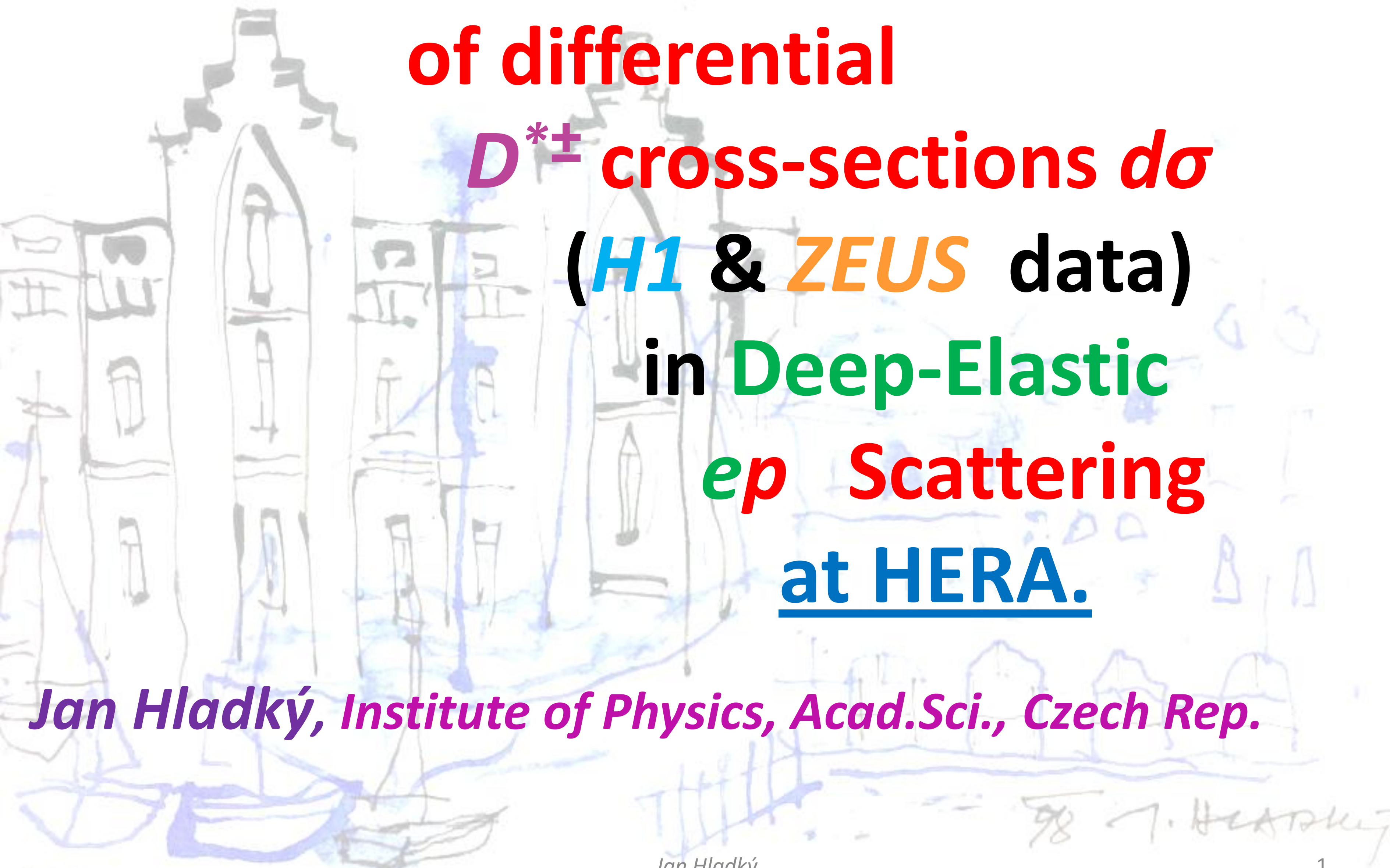

CONTENTS:

1 Introduction
2 Theoretical predictions
3 Data samples for *dσ* combinations
4 Combination method
5 Combined *dσ* cross sections
6 Conclusions

1 Introduction

* DESY in Hamburg → data up to 2007 in *e-p* collider HERA

* experiments *H1* and *ZEUS* → *Fig. 1* studied in *DIS* single and double differential *dσ* in inclusive $D^{*\pm}$ production

* both respective data published

→ new combinations of both data - presented →uncertainties reduction

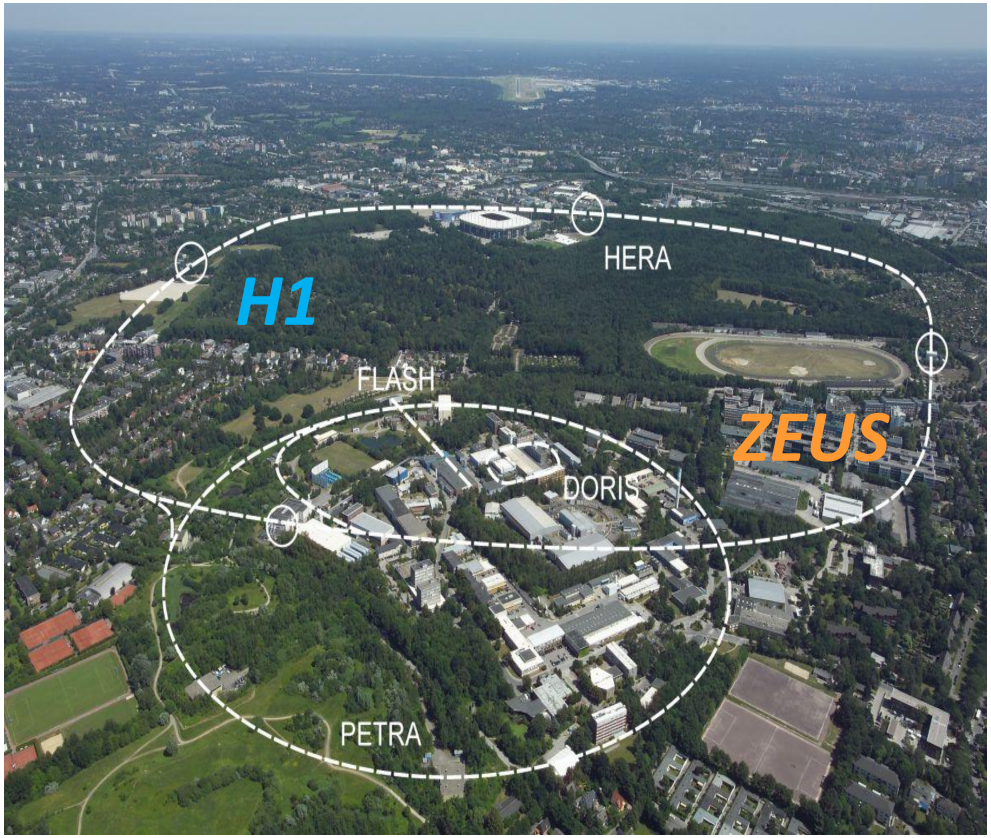

Fig.1 bird's look to DESY

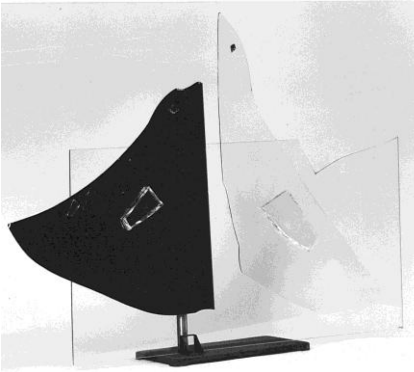

the birds

* Study of *charm production* in *DIS* at HERA

→ stringent perturbative QCD theory tests

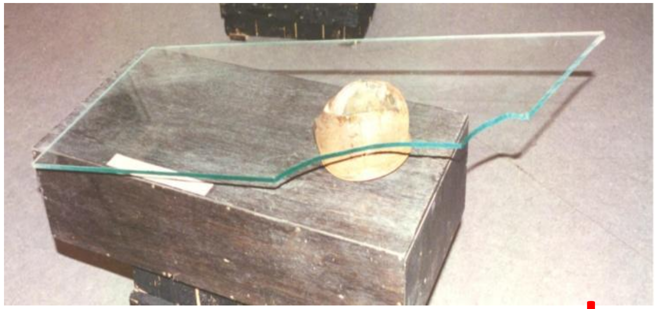

c quark

* charm → dominant gluon-boson fusion

→ sensitive to gluon distribution in proton & sensitivity to c and b quark masses

* measurements - data from HERA-I and HERA-II

==> D° and $D^{*\pm}$ reconstruction

→ directly visible $D^{*\pm}$ # data combination

→ minimal extrapolation

(data have ~ same binning &visible space)

→ to full phase space

* (large extrapolation needs theory assumptions

→ errors & restrictions)

→ comparison with (NLO QCD) predictions

cms energy

$s^{1/2}$= 318 GeV

2 Theoretical predictions

FFNS (Fixed-Flavour-Number-Scheme) - 3-flavour - for NLO calculations and HVQDIS provided NLO QCD ($O(\alpha_s^2)$) for $d\sigma$ predictions for $D^{*\pm}$ production → used

Parameters for prediction's uncertainties estimation:

* renormalisation & factorisation scale $\mu_r = \mu_f = (Q^2+4m_c^2)^{½}$
* pole mass of charm quark m_c = 1.50 ± 0.15 GeV
* strong coupling constant $\alpha_s^{n_f=3}(M_Z)$ = 0.105 ± 0.002
* proton PDFs → described as used in HERAFitter
* fraction f of charm quarks hadronising to $D^{*\pm}$ is 0.2287 ± 0.0056
* fragment. parameter α_K ,bin boundary s_1 , $\langle k_T \rangle$ - as usually varied

For beauty quarks → parameters for predictions uncertainties estimation also calculated. Contribution of beauty hadrons to $D^{*\pm}$ signal is small.

3 Data samples for cross-section combinations

The *H1* and *ZEUS* detectors and their most important components – central tracker (*CTD*)detectors and their electromagnetic sections of the calorimeters *see Fig. 2 and 3.* *CTD* operated inside solenoidal magnetic fields of 1.16 T (*H1*) and 1.43 T (*ZEUS*) and electromagnetic sections of the calorimeters measured charged particles trajectories in polar angular range of $15 < \Theta^\circ < 165$ (164).

For charged particles passing through all Si vertex detectors and *CTDs* → transverse momentum resolutions of $\sigma(p_T)/p_T \sim 0.002 p_T + 0.015$ (*H1*) and $\sim 0.0029 p_T + 0.0081 + 0.0012/p_T$ (*ZEUS*) – (p_T in GeV). Resolution of scattered $e^{\pm}$ electromagnetic energy *E* is: $\sigma(E)/E$ *of* $0.11/E^{1/2}$ in LAr and $0.07/E^{1/2}$ in spacal (*H1*) and $0.18/E^{1/2}$ (*ZEUS*) – *E* in GeV.

Luminosity is known with a precision of 3.2% (*H1*) and ~2% (*ZEUS*).

DETECTORS

H1

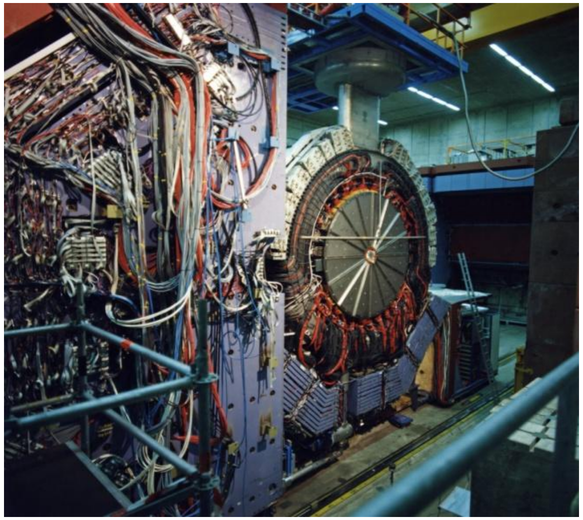

Backw. Pb- fibre scint. elmg. calo

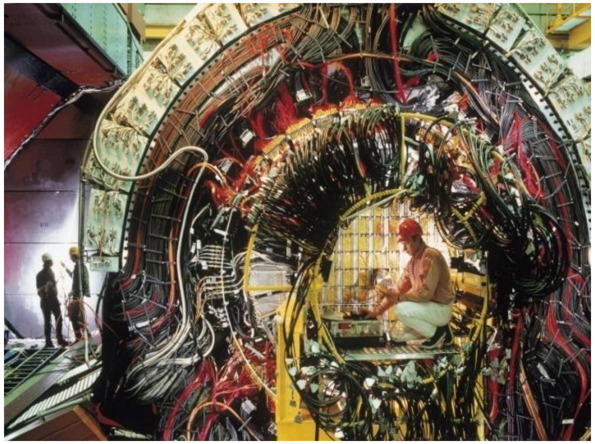

ZEUS

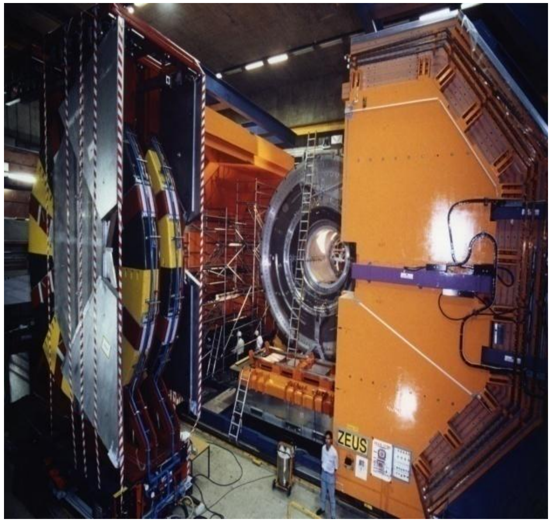

Microvertex detector

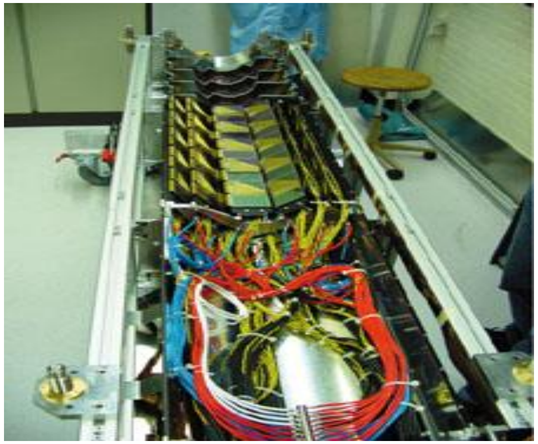

Fig. 2

SPACAL – EM, HAD calo

e

p

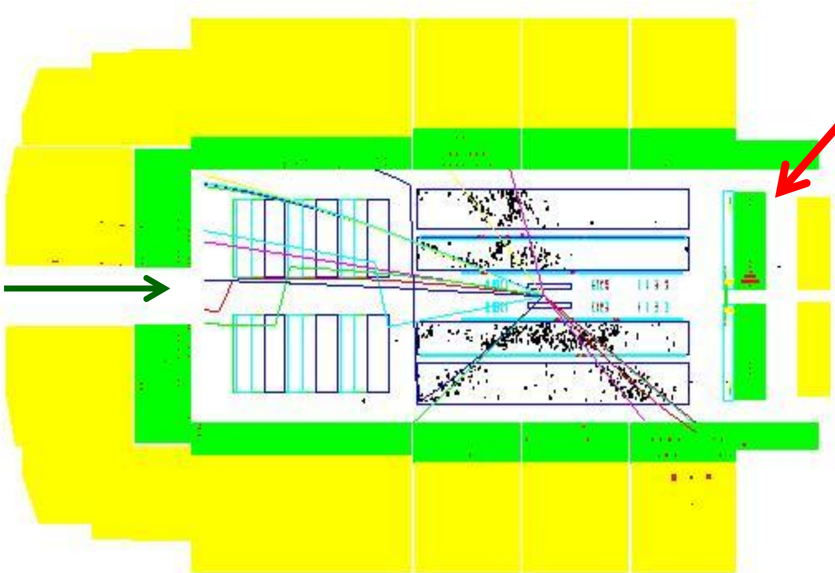

H1

Detector's chart

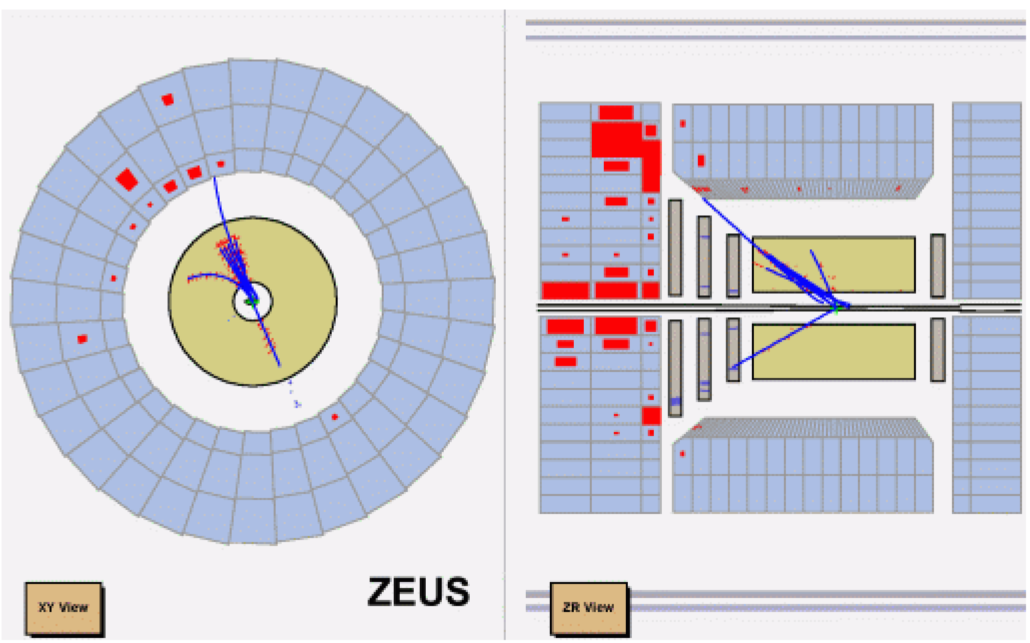

ZEUS

U - calo

Fig. 3

Data sets used for combinations, their kinematic range and luminosity → *Table 1*. $D^{*\pm}$ signal *see Fig. 4 and 5.*

Data set			Kinematic range Q^2 (GeV^2)	y	$p_T(D^*)$ (GeV)	$\eta(D^*)$	$\mathscr{L}$ (pb^{-1})
I	H1 $D^{*\pm}$ HERA-II (medium Q^2)	[18]	5 : 100	0.02 : 0.70	> 1.5	−1.5 : 1.5	348
II	H1 $D^{*\pm}$ HERA-II (high Q^2)	[15]	100 : 1000	0.02 : 0.70	> 1.5	−1.5 : 1.5	351
III	ZEUS $D^{*\pm}$ HERA-II	[20]	5 : 1000	0.02 : 0.70	1.5 : 20.0	−1.5 : 1.5	363
IV	ZEUS $D^{*\pm}$ 98-00 HERA - I	[6]	1.5 : 1000	0.02 : 0.70	1.5 : 15.0	−1.5 : 1.5	82

Tab. 1

Two types of combinations made - for:

a/ single-differential cross section *dσ*

b/ double-differential cross section *dσ*

for a/ - data sets I ÷ III (*see Table 1)* used → combinations for *dσ* (*$D^{*\pm}$*) vs. *p_T* (*$D^{*\pm}$*), pseudorapidity *$\eta(D^{*\pm})$* and inelasticity *$z(D^{*\pm})$* made → *Fig. 6 and 7*

for b/ - all four data sets can be used in combinations and reconstruct *$d\sigma^2/dQ^2dy$* (*$D^{*\pm}$*) → *Fig. 11.*

H1 → $D^{*\pm}$ signal

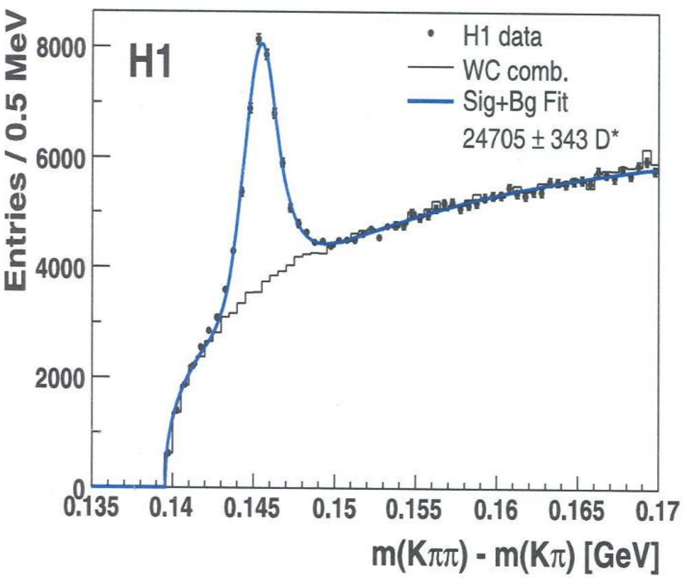

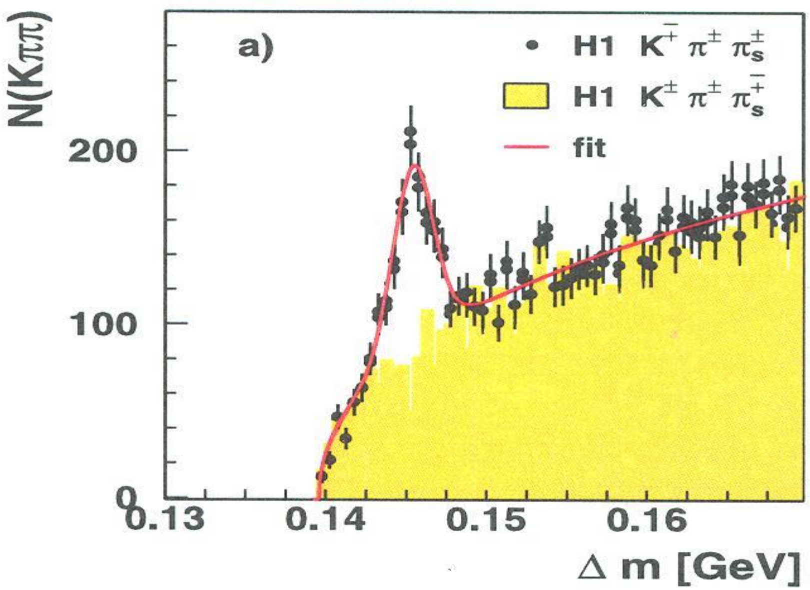

$5 < Q^2 < 100$ GeV^2

$100 < Q^2 < 1000$ GeV^2

Fig. 4

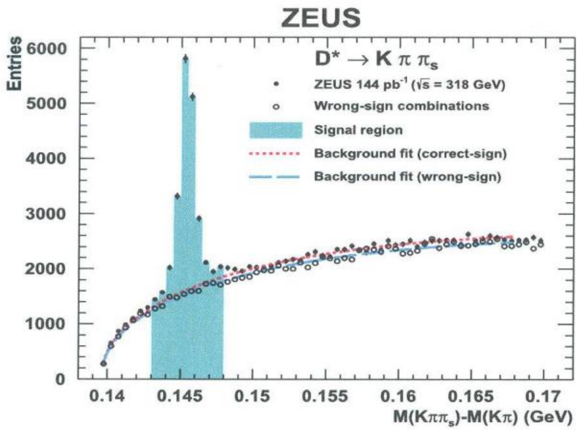

$N(D^*) = 12256 \pm 191$

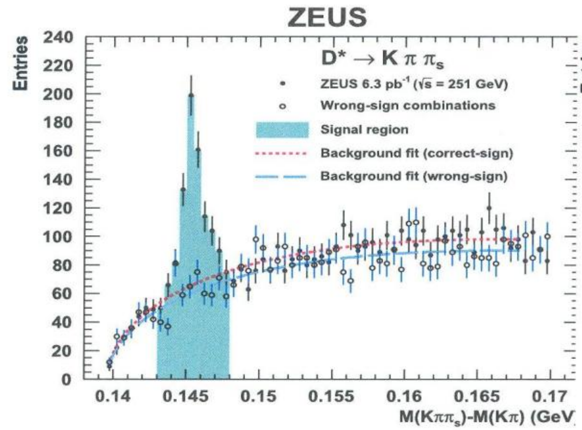

$N(D^*) = 417 \pm 37$

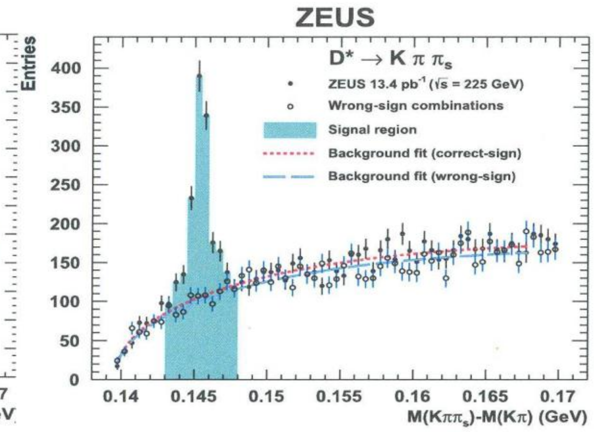

$N(D^*) = 859 \pm 49$

ZEUS (see U. Karshon talk at PHOTON-2015 Conf.)

$D^{*\pm}$ signal

→ **$\sigma(D^{*\pm})$ *grows***

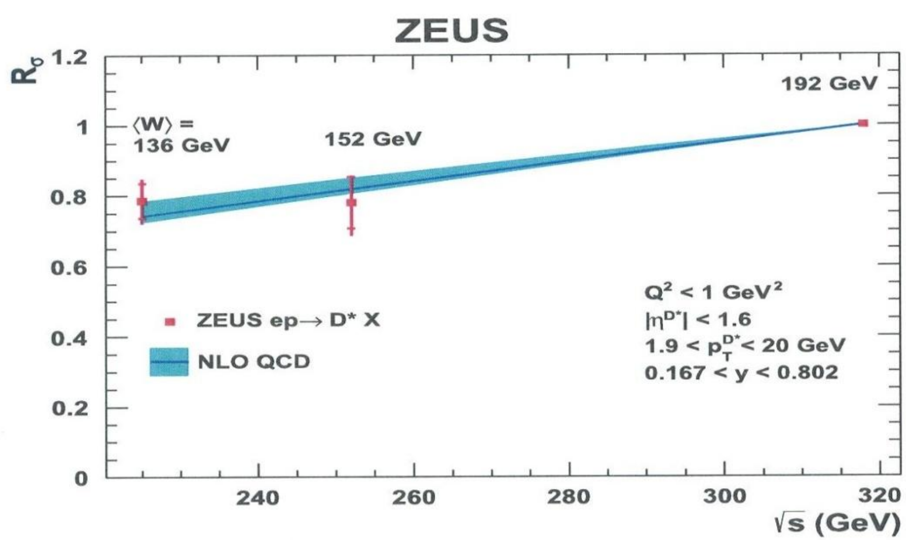

Fig. 5

4 Combination method

* data sets combination uses the χ^2 minimisation method in program HERAverager

* corelated and uncorelated systematic uncertainties fully taken into account

→ are predominantly of multiplicative nature

* statistical uncertainties mostly background dominated

* almost all experimental systematic uncertainties treated as independent between *H1* and *ZEUS* data sets →

$p_T(D^{*\pm})$, $\eta(D^{*\pm})$, $z(D^{*\pm})$, Q^2, y *not* statistically independent

→ each combined separately

* for $d\sigma$ combinations - theory uncertainties → 0 – 10% of total

* several $d\sigma$ intervals were combined using shape HVQDIS predictions program

* inner error bars – uncorrelated part of uncertainties,
outer error bars – total uncertainties,

histogram shows the binning for *dσ* calculation.

* the bottom part shows the ratio of *dσ* with respect to central value of combined *dσ*.

Combined *H1* & *ZEUS* data

$d\sigma/dp_T(D^{*\pm})$

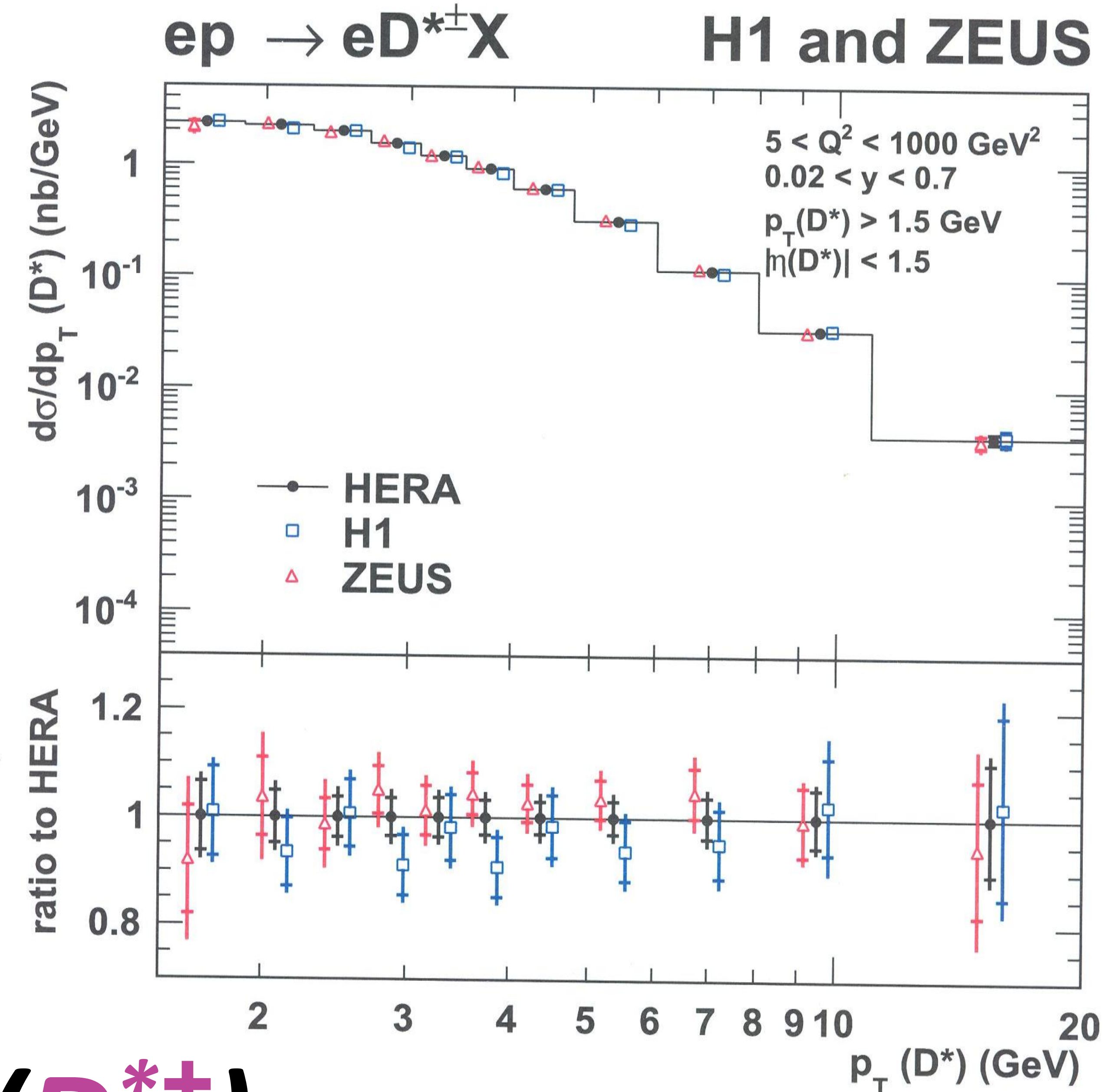

Fig. 6

<u>inner</u> error bars – **uncorrelated** part of uncertainties, <u>outer</u> error bars – **total** uncertainties

Combined

H1 & *ZEUS* data

$d\sigma/dz\ (D^{*\pm})$

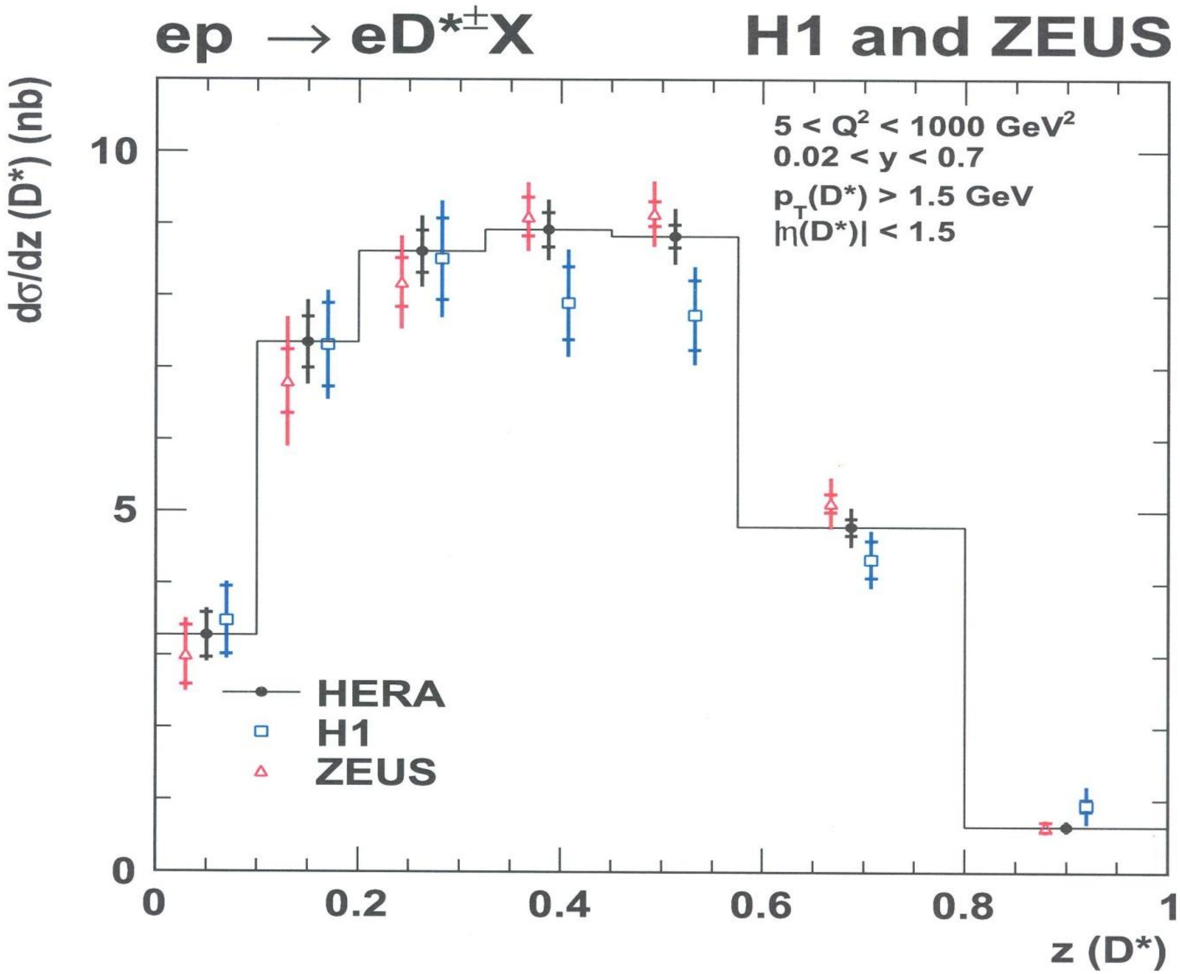

Fig. 7

Combined

H1 & *ZEUS*
data
compared to
NLO QCD
predictions

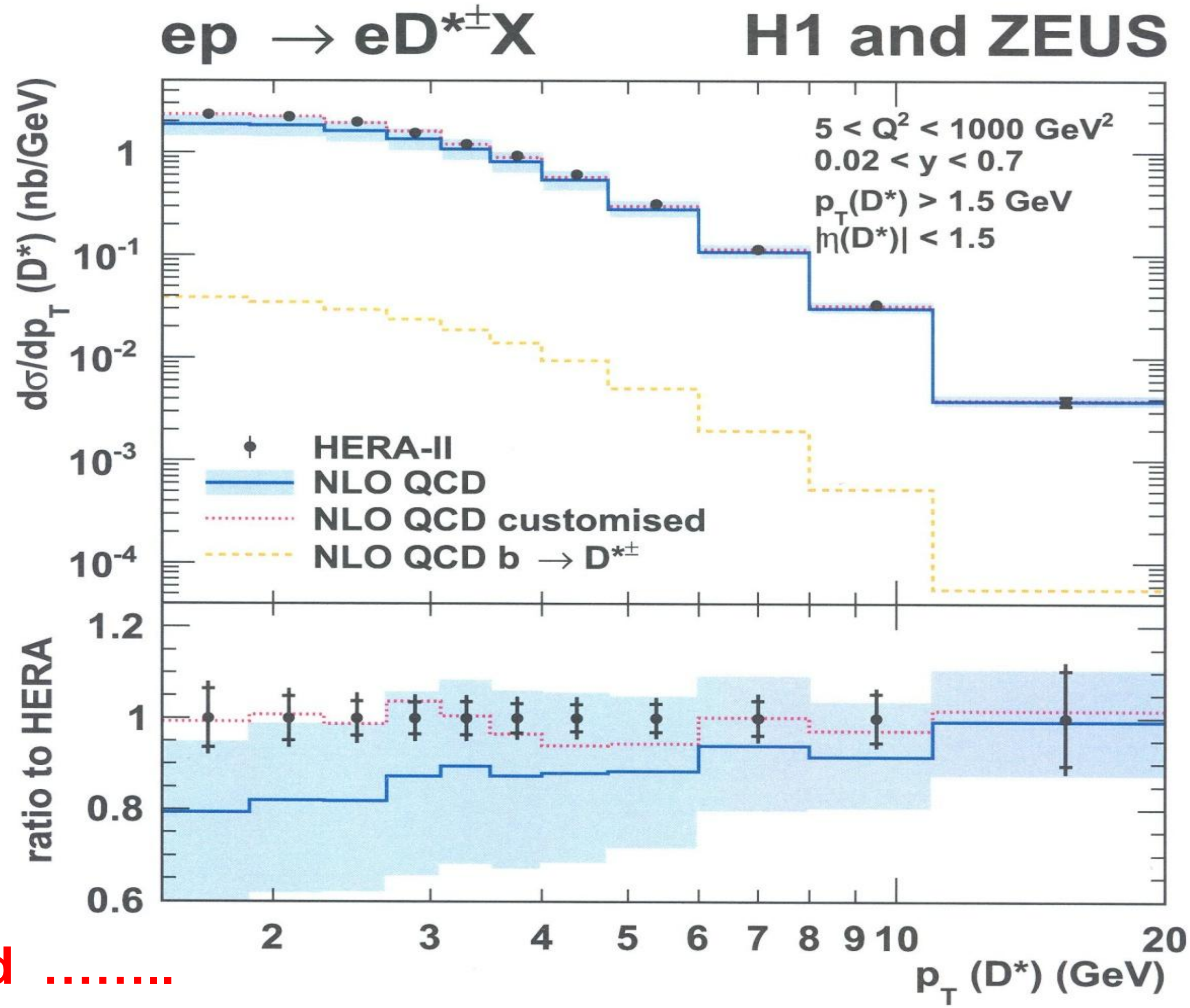

NLO QCD customized ……..

$d\sigma/dp_T(D^{*\pm})$

Fig. 8

Combined

H1 & *ZEUS* data

compared to

NLO QCD predictions

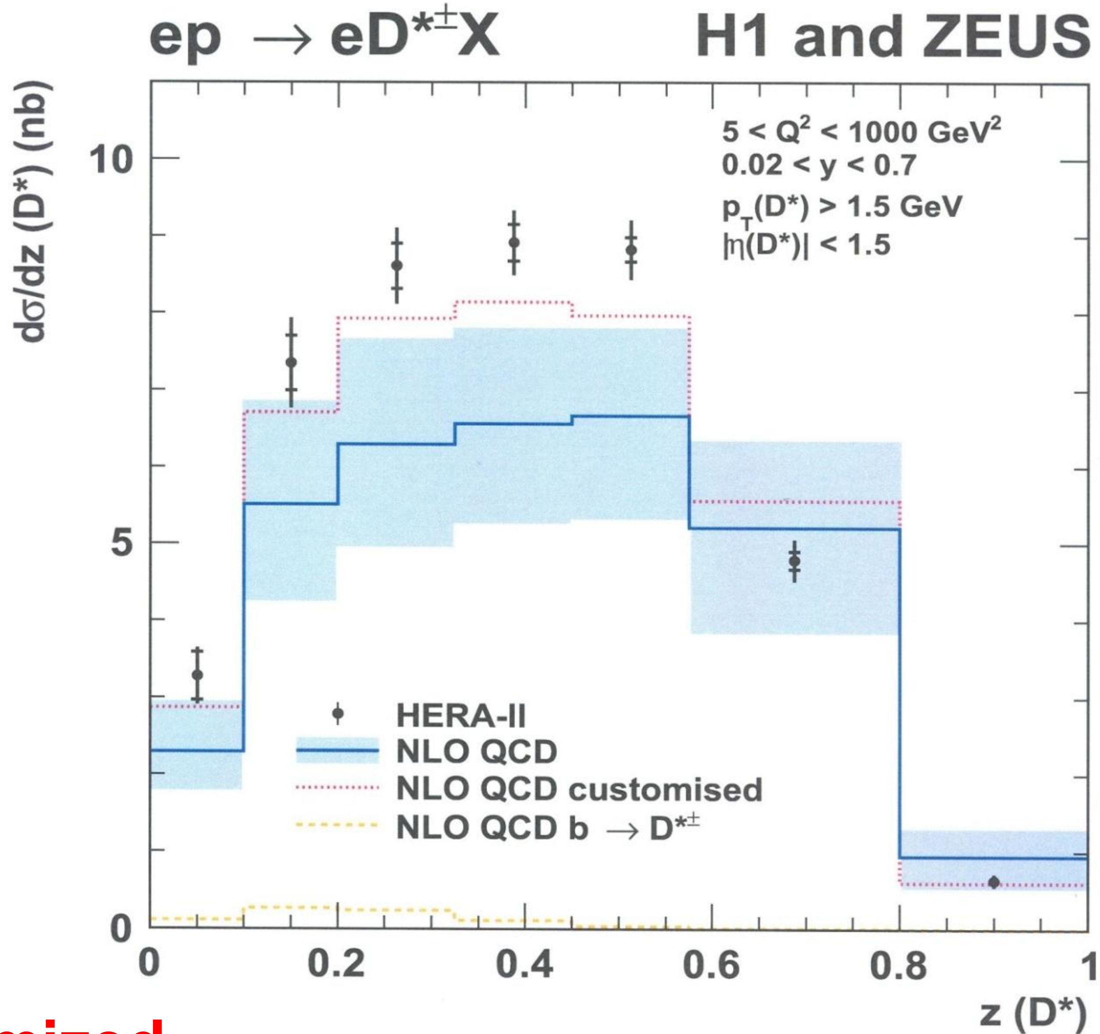

NLO QCD customized ……..

$d\sigma/dz\ (D^{*\pm})$

Fig. 9

5 Combined cross sections

* combinations for $d\sigma$ ($D^{*\pm}$) vs. p_T ($D^{*\pm}$), and inelasticity $z(D^{*\pm})$ from HERA II data made, *see Fig. 6 and 7* → ***dataset consistent***

* comparision to NLO QCD - HVQDIS predictions, *see Fig. 8 and 9*

*→ *fits O.K.*

→ but NLO customization *fits better!*

* precision - data ~ 5%, theory ~ 30% low Q^2 → 10% high Q^2

==

* NLO customization → *precise study theory uncertainties*

set pole mass m_c = *1.35 GeV* or

reduce or increase μ_r and μ_f *scale by factor 2 - see FIG. 10*

→ describes data very well → *new* way for future theory

→ NNLO calculations & improved fragmentation models may help

→ similar conclusions valid also for $d\sigma^2/dQ^2dy(D^{*\pm})$ combinations

Ratios:
NLO predictions
to HERA data
for
various m_c , $\mu_r = \mu_f$

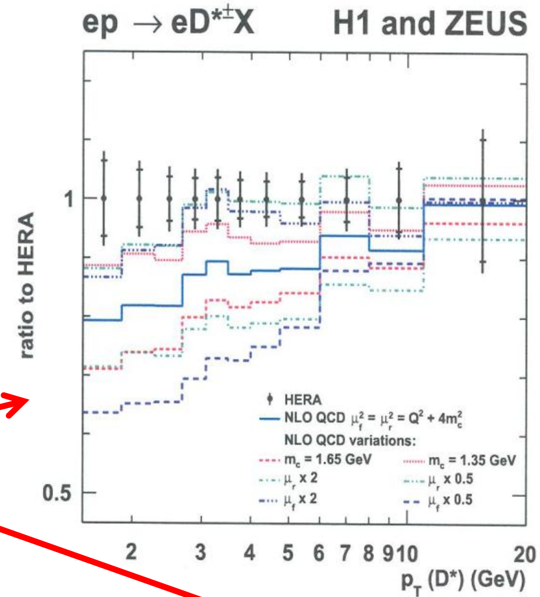

vs. p_T ($D^{*\pm}$)

for fragmentation bin boundary s_1

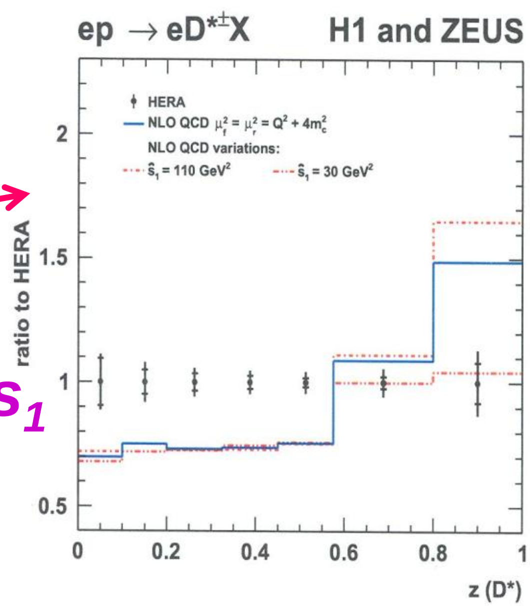

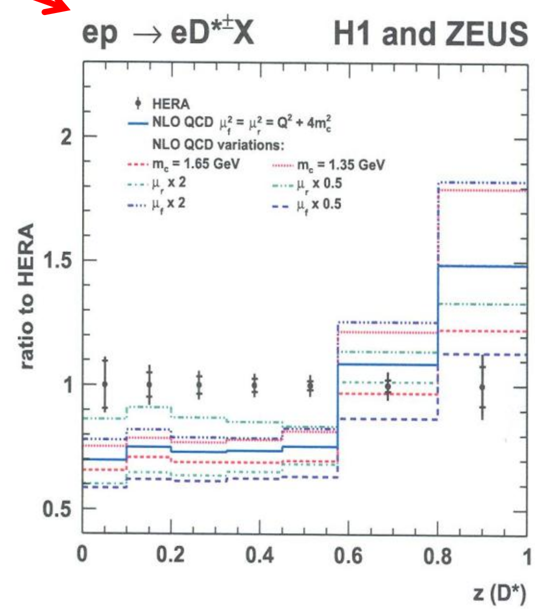

vs. z ($D^{*\pm}$)

Fig. 10

H1(HERA-II) □
ZEUS (HERA-I ○
and *HERA-II)* △
data & common
combinations ●

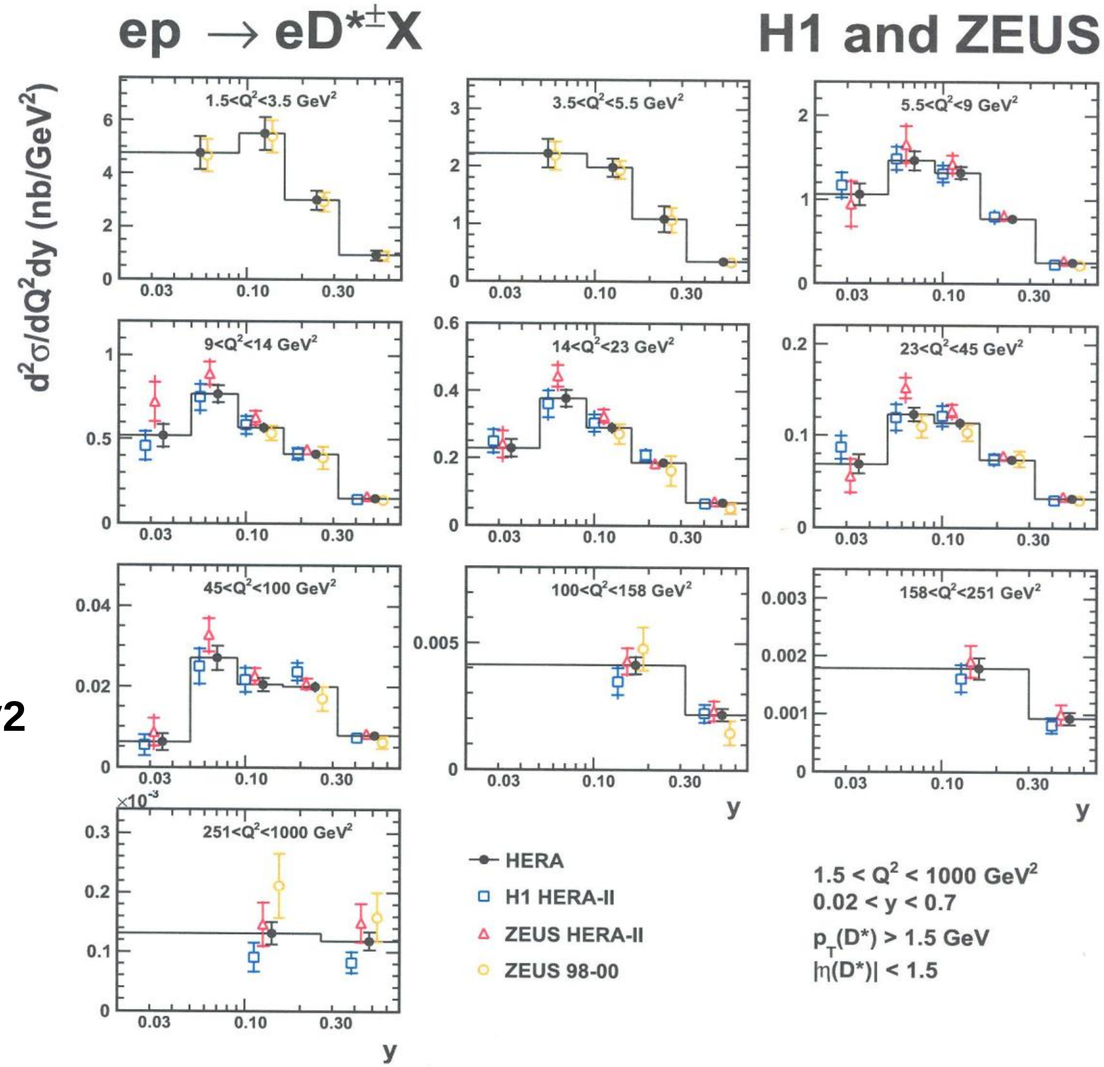

$1.5 < Q^2 < 1000$ GeV^2
$0.02 < y < 0.7$
p_T $(D^{*\pm})$ > 1.5 GeV
$|\,\eta(D^{*\pm})\,| < 1.5$

$d\sigma^2/dQ^2dy(D^{*\pm})$

Fig. 11

Combined
H1 & ZEUS
data
compared to
NLO QCD
predictions

$1.5 < Q^2 < 1000$ GeV^2
$0.02 < y < 0.7$
$p_T\,(D^{*\pm}) > 1.5$ GeV
$|\,\eta(D^{*\pm})\,| < 1.5$

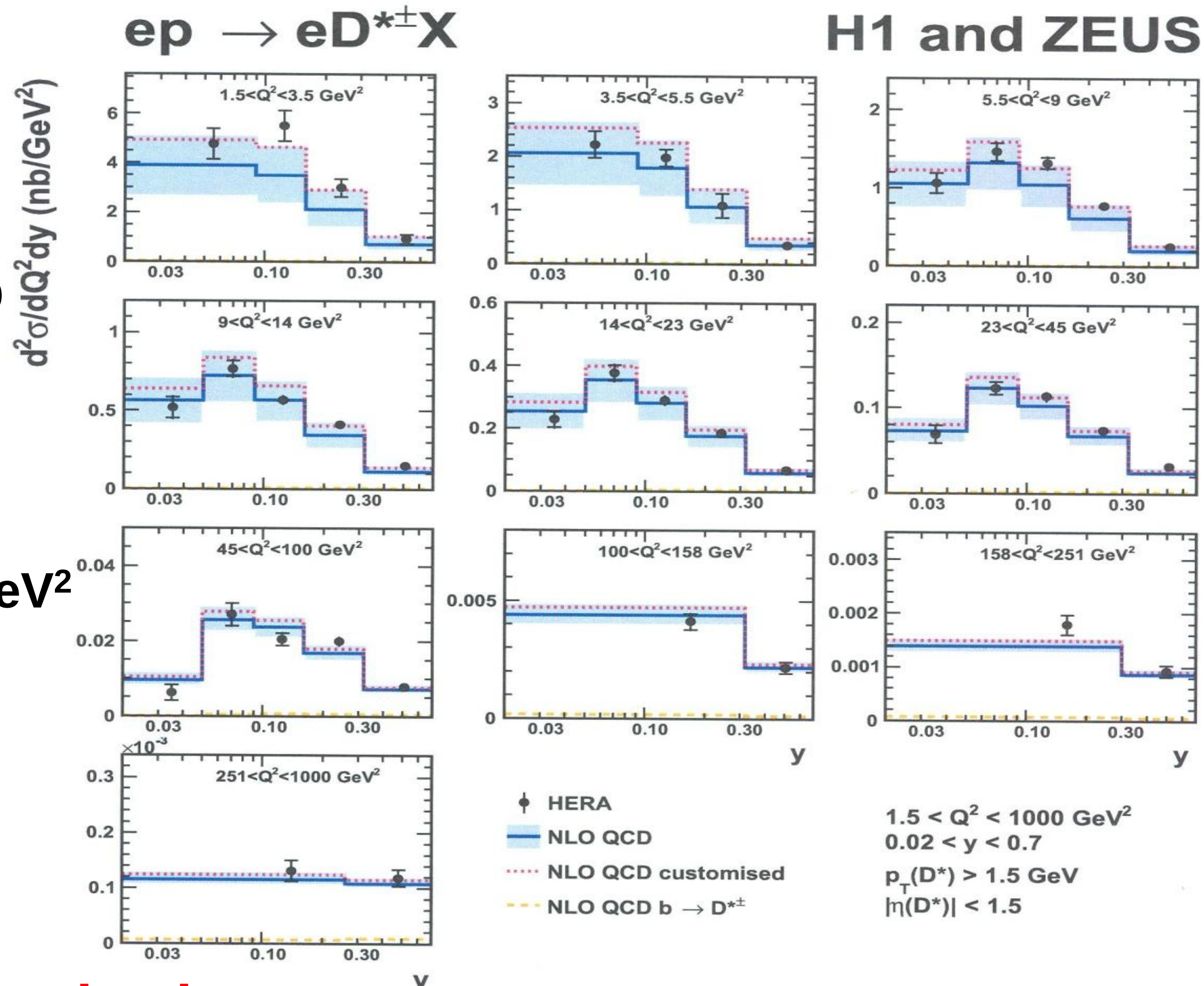

HERA ●

NLO QCD customized ……..

$d\sigma^2/dQ^2dy(D^{*\pm})$

Fig. 12

6 Conclusions

* $D^{*\pm}$ - production cross-section data in *e-p* DIS in *H1* and *ZEUS* exp. combined at the level of visible ## → accounting for their systematic correlations.

* data sets were consistent and the combination reduced significantly their uncertainties.

* combination has no significant theory-related uncertainties.

* several kinematic variables of $D^{*\pm}$ are presented.

* combined data are compared to NLO QCD.

* NLO predictions describe data o.k. within their uncertaint.

* Higher order calculations could help to reduce theory uncertainties nearer to experimental data precision.

* Further improvements in heavy-quark fragmentation treatment are desirable.

Thanks,

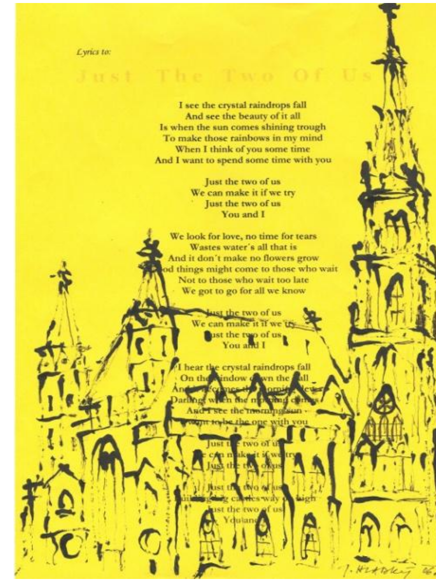

St. Stephan

enjoy

Wien

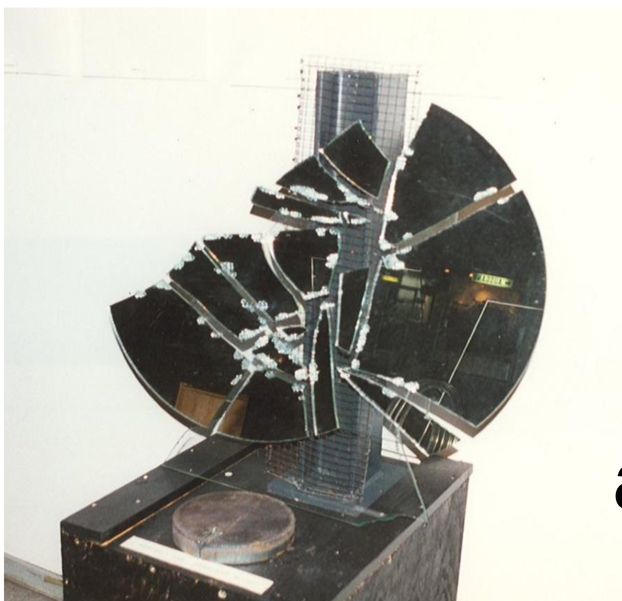

and think on new discoveries!

supersymmetric particle

B A C K U P

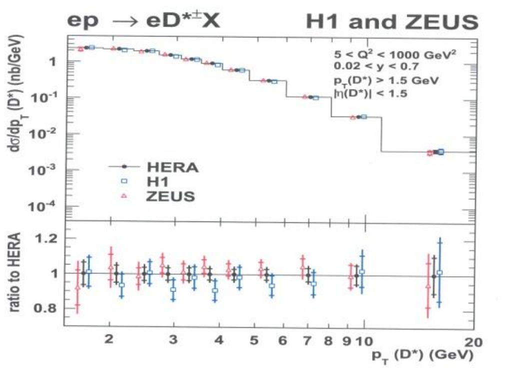

Figure 1: Differential $D^{*\pm}$-production cross section as a function of $p_T(D^*)$. The open triangles and squares are the cross sections before combination, shown with a small horizontal offset for better visibility. The filled points are the combined cross sections. The inner error bars indicate the uncorrelated part of the uncertainties. The outer error bars represent the total uncertainties. The histogram indicates the binning used to calculate the cross sections. The bottom part shows the ratio of these cross sections with respect to the central value of the combined cross sections.

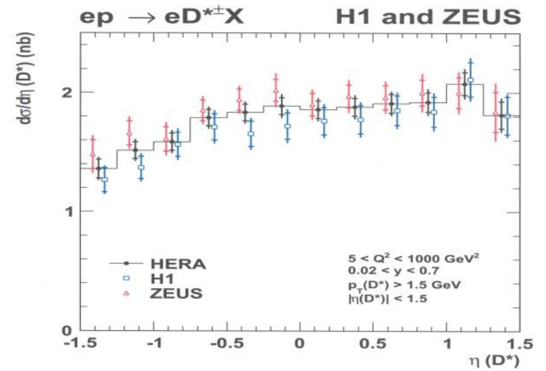

Figure 2: Differential $D^{*\pm}$-production cross section as a function of $\eta(D^*)$. The open triangles and squares are the cross sections before combination, shown with a small horizontal offset for better visibility. The filled points are the combined cross sections. The inner error bars indicate the uncorrelated part of the uncertainties. The outer error bars represent the total uncertainties. The histogram indicates the binning used to calculate the cross sections.

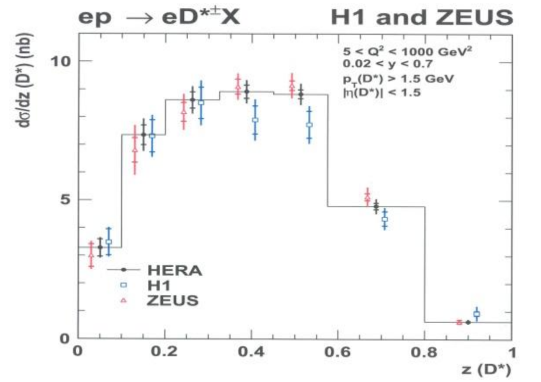

Figure 3: Differential $D^{*\pm}$-production cross section as a function of $z(D^*)$. The open triangles and squares are the cross sections before combination, shown with a small horizontal offset for better visibility. The filled points are the combined cross sections. The inner error bars indicate the uncorrelated part of the uncertainties. The outer error bars represent the total uncertainties. The histogram indicates the binning used to calculate the cross sections.

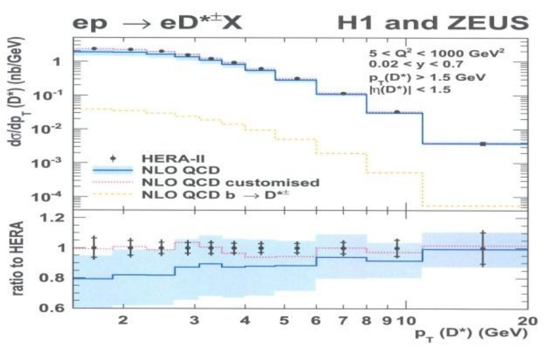

Figure 6: Differential $D^{*\pm}$-production cross section as a function of $p_T(D^*)$. The data point are the combined cross sections. The inner error bars indicate the uncorrelated part of th uncertainties. The outer error bars represent the total uncertainties. Also shown are the NL(predictions from HVQDIS (including the beauty contribution) and their uncertainty band. / customised NLO calculation (dotted line, see text) is also shown. The bottom part shows th ratio of these cross sections with respect to the central value of the combined cross sections.

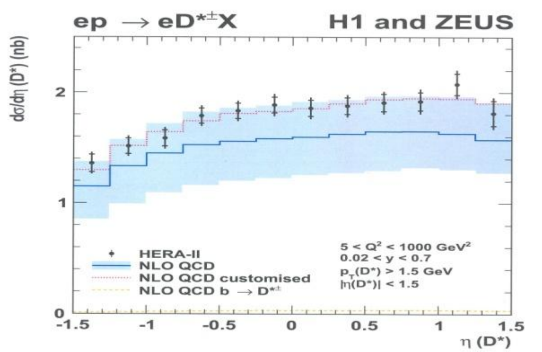

Figure 7: Differential $D^{*\pm}$-production cross section as a function of $\eta(D^*)$. The data points are the combined cross sections. The inner error bars indicate the uncorrelated part of the uncertainties. The outer error bars represent the total uncertainties. Also shown are the NLO predictions from HVQDIS (including the beauty contribution) and their uncertainty band. A customised NLO calculation (dotted line, see text) is also shown.

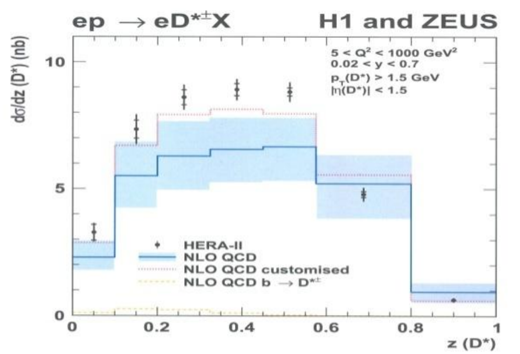

Figure 8: Differential $D^{*\pm}$-production cross section as a function of $z(D^*)$. The data points are the combined cross sections. The inner error bars indicate the uncorrelated part of the uncertainties. The outer error bars represent the total uncertainties. Also shown are the NLO predictions from HVQDIS (including the beauty contribution) and their uncertainty band. A customised NLO calculation (dotted line, see text) is also shown.

BACKUP

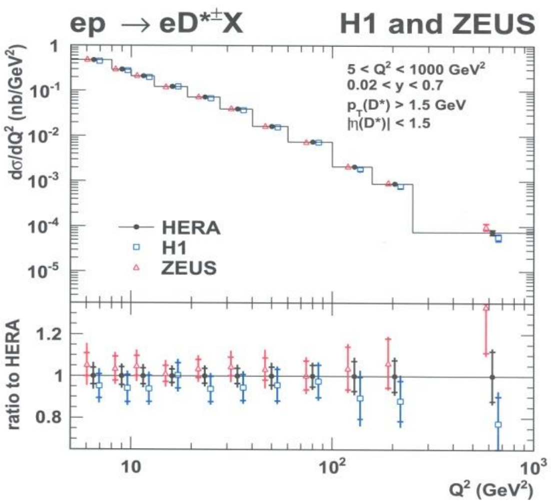

Figure 4: Differential $D^{*\pm}$-production cross section as a function of Q^2. The open triangles and squares are the cross sections before combination, shown with a small horizontal offset for better visibility. The filled points are the combined cross sections. The inner error bars indicate the uncorrelated part of the uncertainties. The outer error bars represent the total uncertainties. The histogram indicates the binning used to calculate the cross sections. The bottom part shows the ratio of these cross sections with respect to the central value of the combined cross sections.

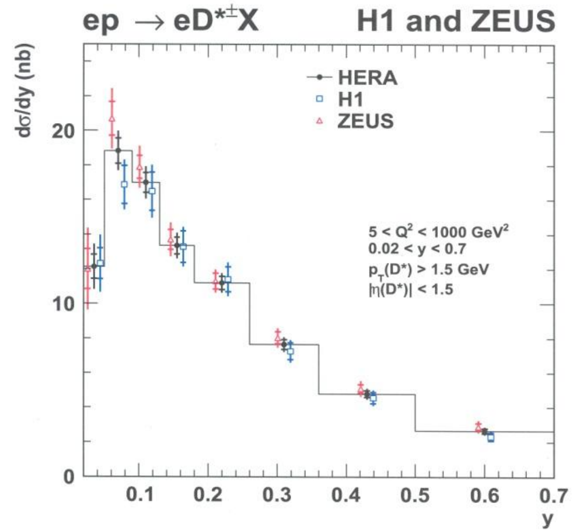

Figure 5: Differential $D^{*\pm}$-production cross section as a function of y. The open triangles and squares are the cross sections before combination, shown with a small horizontal offset for better visibility. The filled points are the combined cross sections. The inner error bars indicate the uncorrelated part of the uncertainties. The outer error bars represent the total uncertainties. The histogram indicates the binning used to calculate the cross sections.

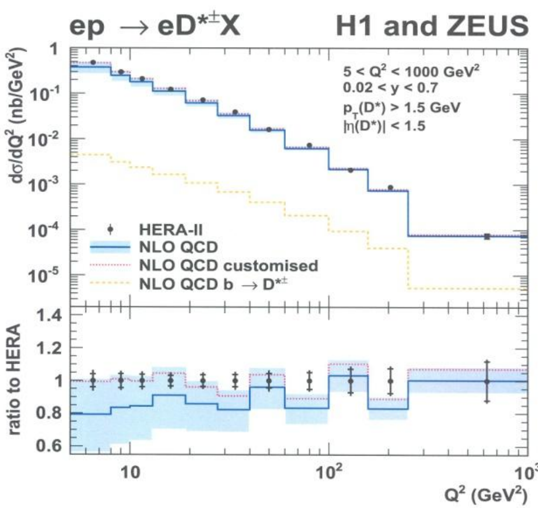

Figure 9: Differential $D^{*\pm}$-production cross section as a function of Q^2. The data points are the combined cross sections. The inner error bars indicate the uncorrelated part of the uncertainties. The outer error bars represent the total uncertainties. Also shown are the NLO predictions from HVQDIS (including the beauty contribution) and their uncertainty band. A customised NLO calculation (dotted line, see text) is also shown. The bottom part shows the ratio of these cross sections with respect to the central value of the combined cross sections.

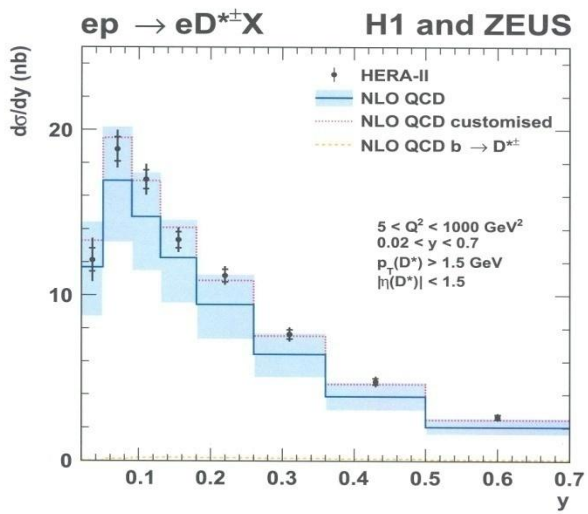

Figure 10: Differential $D^{*\pm}$-production cross section as a function of y. The data points are the combined cross sections. The inner error bars indicate the uncorrelated part of the uncertainties. The outer error bars represent the total uncertainties. Also shown are the NLO predictions from HVQDIS (including the beauty contribution) and their uncertainty band. A customised NLO calculation (dotted line, see text) is also shown.